Istraživanja I projektovanja za privredu
ISSN 1451-4117
DOI:10.5937/jaes0-63201
www.engineeringscience.rs

iipp publishing

Journal of Applied Engineering Science
Professional Paper,
Volume 24, Number 4, Year 2026,
no 1359, pp 636-647

INFLUENCE OF LOCALIZED CORROSION DAMAGE OF REINFORCEMENT ON BONDING WITH CONCRETE

Dmitriy Popov*, Maksim Kudryavtsev

Moscow State University of Civil Engineering, Institute of Industrial and Civil Engineering, Department of Reinforced Concrete and Masonry Structures, Moscow, Russia

**popovds@mgsu.ru*

The most common defect in reinforced concrete structures is corrosion damage to the working reinforcement in the concrete body. The main danger of corrosion damage is caused by several factors: increase of corrosion products in the volume and creation of additional tensile stresses in concrete along the length of the bar, which leads to spalling of the concrete cover; reduction in the diameter of the working reinforcement; areas of local bare reinforcement due to the destruction of the concrete cover. There are many methods for assessing the stress-strain state of damaged structures, but for each type of damage it is worth introducing certain refinements to the calculation methods. The paper presents the analysis of domestic and foreign literature on the assessment of reinforcement bonding with concrete, the results of tests carried out by the authors of the article to assess the loss of bonding of corrosion-damaged reinforcing bars in the body of concrete.

Keywords: reinforced concrete, reinforcement-concrete bond, experimental studies, numerical studies

HIGHLIGHTS

- Pull-out tests show that 23 % cross-section loss reduces bond strength by 6 % while increasing steel stress by 6.8 %.
- Corrosion products alter the bond mechanism: friction governs the slip response, eliminating the plastic plateau seen in uncorroded bars.
- A finite-element model with nonlinear COMBIN39 springs calibrated from experiments accurately reproduces the pull-out load–slip curves.
- Numerical analysis reveals that corrosion reduces both anchorage capacity and bar deformations, with 6.6 times smaller end displacement.

1 Introduction

Bond between reinforcing steel and concrete is a fundamental factor governing the composite action of reinforced concrete as a monolithic structural element. Deterioration of bond results in extensive cracking, reduced flexural stiffness, and diminished load-bearing capacity of the member as a whole. Since the advent of reinforced concrete, extensive research has been devoted to bond behavior, and it has been established that bond stresses are influenced by concrete tensile strength, bar diameter, surface geometry (rib pattern), loading regime, and other parameters.

However, the vast majority of classical bond-slip relationships are derived for uncorroded reinforcement. In actual service conditions, the most pervasive and critical defect is corrosion of the main reinforcement embedded in concrete. Corrosion not only reduces the effective cross-sectional area of the bar but also generates a layer of corrosion products at the steel–concrete interface, which fundamentally alters the friction mechanism and disrupts bond integrity. Consequently, there is a clear need to refine existing analytical models to adequately account for the specific behavior of corroded reinforcement.

The objective of the present study is twofold: to experimentally and numerically quantify the loss of bond between corroded reinforcing bars and concrete, and to verify a novel numerical approach that simulates the interfacial interaction via nonlinear spring elements, capable of accurately reproducing the pull-out load–slip response.

Within this framework, the following tasks are addressed:

- Pull-out testing of both control and corroded specimens with a fixed corrosion level, in order to obtain reliable reference data for model calibration.
- Development of a finite-element model that emulates bond degradation through nonlinear springs, the stiffness characteristics of which are derived from experimental results.

The methodology relies on physical experimentation (electrochemically induced corrosion with controlled sectional loss) followed by numerical simulation using the Ansys software package. The choice of a fixed corrosion degree (23 % in terms of cross-sectional area reduction) is deliberate, being dictated by the need to calibrate and validate the numerical approach at this initial stage. Parametric variation of corrosion level, bar diameter, and concrete strength class is scheduled as a subsequent phase of the research

Over the past decades, a substantial body of experimental and analytical research has been devoted to the bond between reinforcing steel and concrete, leading to the development of numerous empirical and semi-empirical

relationships [4–23]. Table 1 summarizes the most representative and widely cited models proposed for uncorroded reinforcement. Table 1 provides an overview of techniques for determining the bond between reinforcement and concrete.

Table 1. Methods for determining the bond between reinforcement and concrete

Authors	A literary source	Method of calculation
Kholmianskiy M.M.	[4]	$\tau = B\frac{\ln(l+as)}{l+as}$, where $B = e\tau_{max}$ and $a = \frac{e-l}{s_{max}}$ coefficients accepted on the basis of experimental studies.
Shima H., Chou L.-L., Okamura H. Micro and Macro Models	[5]	$\tau = B\frac{[\ln(l+as)]^3}{l+\beta s}$
Balázs G.L.	[6]	$\tau = \tau_{max}\frac{2s_{max}s}{s_{max}^2+s^2}$
CEB-FIP Model Code 90	[7]	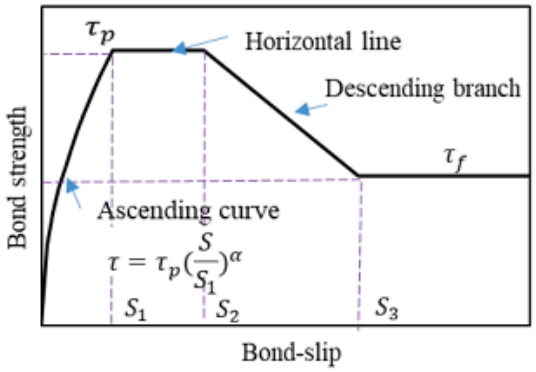 $\tau = \begin{cases} \tau_{max}\left(\frac{s}{s_1}\right)^a, 0 \le s < s_1; \\ \tau_{max}, s_1 \le s < s_2; \\ \tau_{max} + (\tau_f - \tau_{max})\left(\frac{s-s_2}{s_3-s_2}\right), s_2 \le s < s_3; \\ \tau_f, s > s_3; \end{cases}$ where τ_{max} and τ_f are the maximum and residual bond stress, respectively; s_1, s_2, and s_3 are the slips at different turning points of the bond-slip curve; and α is an index controlling the shape of the ascending part of the curve.
Cruz J.S., Barros J.	[8]	$\tau = \begin{cases} \tau_{max}\left(\frac{s}{s_{max}}\right)^a, & s \le s_{max} \\ \tau_{max}\left(\frac{s}{s_{max}}\right)^{-a'}, & s > s_{max} \end{cases}$ Modification CEB-FIP Model Code 90, taking into account the nonlinear character of the descending branch of the diagram.
G. Rehm	[9]	$\tau = c_1 s^a + c_2 s$, where τ, s - the bond stress and the relative slip between reinforcement and concrete, respectively; c_1, c_2 and a are experimentally identified coefficients.
ACI Committee 318	[21]	$f_b = \frac{2\mu}{\pi}\sigma_n + f_{adh} = \frac{2\mu}{\pi}(\sigma_c + \sigma_{st} + \sigma_{conf}) + f_{adh}$ $f_b = \beta\sigma_n + f_{adh}$ where bond strength f_b, quantified herein as an average shear stress acting on the lateral surface of the bar is, apart from initial adhesion f_{adh}, proportional to the normal confining pressure mobilized on the bar over the anchorage. The normal confining pressure σ_n comprises contributions from the hoop stresses of the concrete cover σ_c, the reaction of stirrups as they

Authors	A literary source	Method of calculation
		cross the splitting plane σ_{st} (calculated as the average normal compressive stress in reaction to the stirrup tensile forces), and any transverse compressive stress field σ_{conf} existing in the anchorage zone. Thus, the values of the term β taken from the international literature correspond to the product 2μ/π.
SP 63.13330	[23]	$R_{bond} = \eta_1 \cdot \eta_2 \cdot R_{bt}$ Where η_1 - coefficient that considers the influence of the type of reinforcement surface; η_2 - coefficient considering the reinforcement bar diameter; R_{bt} - axial tensile strength of concrete.

However, a critical review of the above relationships reveals that none of them explicitly accounts for the presence of corrosion products at the steel–concrete interface, nor for the associated modification of the interfacial interaction mechanics. It is precisely this circumstance that necessitates the present study, aimed at quantitative assessment of bond loss due to corrosion-induced damage.

2 Materials and methods

2.1 Experimental research methods

To evaluate the bonding of reinforcement with concrete, an experiment was set up based on Moscow State University of Civil Engineering. Reinforcement bars 400 mm long, 8 mm diameter of class A500C were concreted in cubes of strength class B25 [23]. The working part of the bar having bond with concrete is five diameters of rebar (40 mm). The rest of the reinforcing bar is isolated from the concrete using a plastic sleeve.

Two specimens were produced. The first series is control, the second series have corrosion damage of the reinforcing bar.

Corrosion of the reinforcement was created by electrochemical corrosion. The specimens were placed in a plastic container and filled with 5% NaCl solution. Using a constant current controller, a positive charge was applied to the reinforcement bar, and a negative charge was applied to the salt solution. The corrosion process at a constant current of 0.5A took 60 days. The diameter of the reinforcement before corrosion determined by weighing was 8.12 mm (As=0.52 cm^2). After corrosion, the diameter (was measured with a vernier caliper) of the reinforcement was 7.14 mm ($A_{s,cor}$=0,40 cm^2), percentage of corrosion of reinforcement in the concrete body by diameter $\Delta_D = \frac{(D_s - D_{s,cor})}{D_s} \cdot 100\% = \frac{(0{,}812 - 0{,}714)}{0{,}812} \cdot 100 = 12{,}07\%$ and by cross-sectional area $\Delta_A = \frac{(A_s - A_{s,cor})}{A_s} \cdot 100\% = \frac{(0{,}52 - 0{,}40)}{0{,}52} \cdot 100 = 23{,}08\%$. The scheme of testing of specimens is presented in Figures 1, 2.

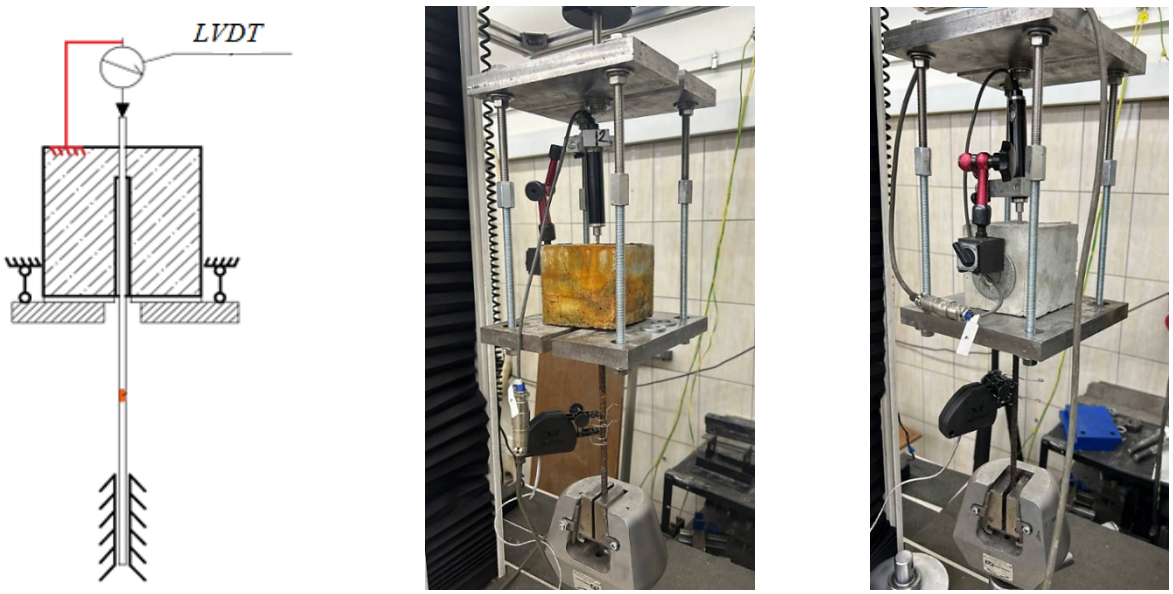

a) test pattern b) sample with corrosion c) sample without corrosion

Fig. 1. Schematic of the test

Based on the results of the tests, the obtained averaged data were analyzed and plots of the displacement of the free end of the reinforcing bar from the applied external load were drawn. The reinforcement stubble slip graphs are shown in Figures 2 and 3.

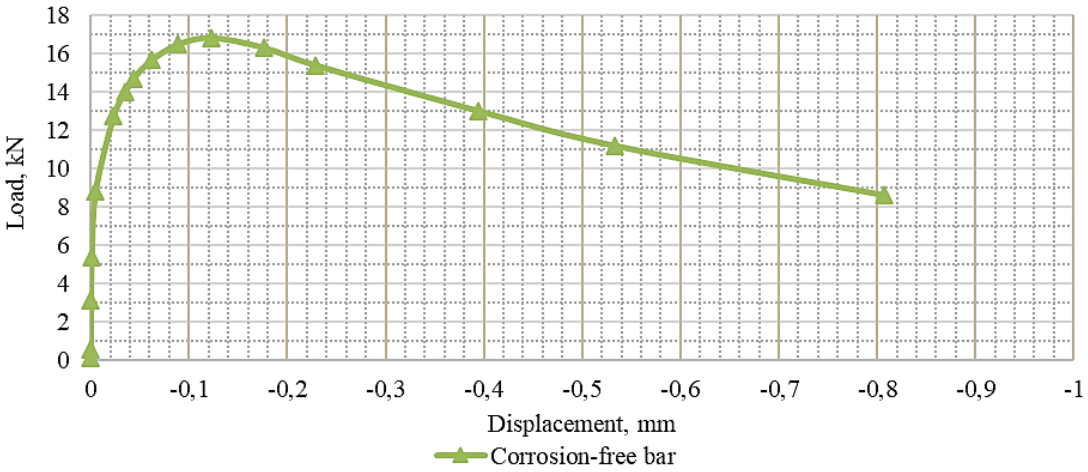

Fig. 2. Bonding of reinforcement prior to corrosion

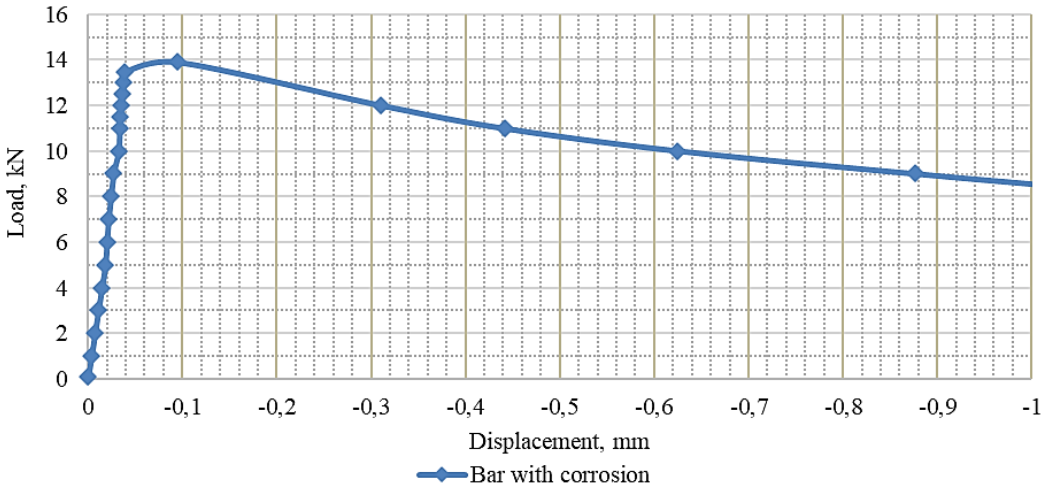

Fig. 3. Bonding of reinforcement after corrosion

The relative anchorage length of the uncorroded rod was 40 mm / 8.12 mm = 4.93, for the corrosion-damaged one considering the reduced diameter 40 mm / 7.14 mm = 5.6. As can be seen from the deformation diagrams, the non-corroded rod slips at higher axial load and has a smoother deformation pattern without sharp drops in the graph. The specimen with corrosion damage (Figure 3) has a linear deformation plot with no curvature almost up to the peak load.

The explanation for this behavior of specimens in the graph can be due to the loss of bond between the rod and concrete. In Figure 2, at a load of 8 kN, there is a slight fracture after which the angle of inclination of the graph to the horizontal axis changes. At this point, the tensile stress in the concrete at the point of contact with the reinforcement profile becomes nonlinear in the concrete deformation graph.

For the series of specimens with bond damage, there is no such fracture, which is explained by the friction of the rod against the corrosion products that are held by adhesion in the concrete body. Nonlinearity is evident at 0.9 of the maximum loads.

We plot the deformation in the axes " Stress-displacement relationship of bar end " (Figure 4). Bond stresses from experimental data are determined by formula 1:

$$\tau = \frac{N}{l \cdot \pi \cdot d} \tag{1}$$

where N - axial load on the bar; l - anchoring length of the bar in concrete; d - bar diameter.

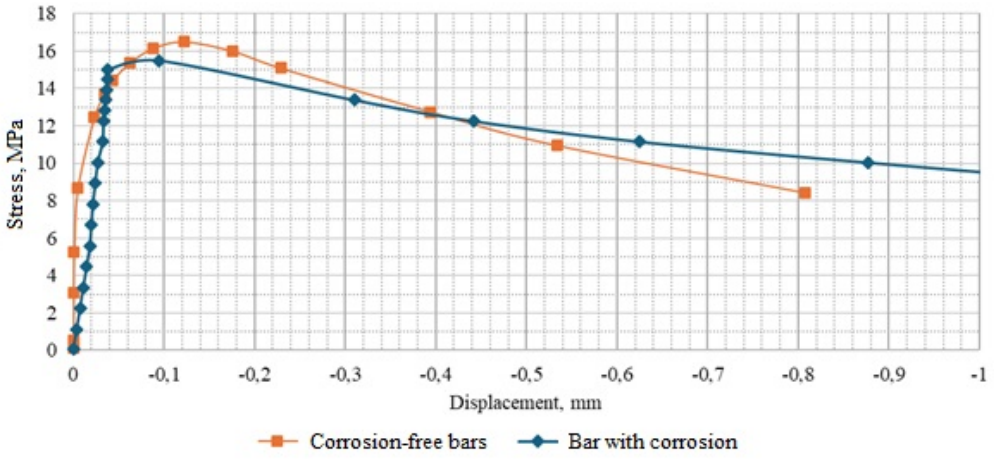

Fig. 4. Diagram of the test results

Table 2 shows the main parameters obtained from the test results. Figures 5, 6 show the samples after fracture.

Table 2. Test results

Type of sample	Bar diameter, mm	Maximum load, kN	τmax, MPa	Stress in the bar σ, MPa	Δτ, %	Δσ, %
With corrosion	7,14	13,89	15,5	347,3	6,05	6,84
No corrosion	8,12	16,83	16,5	325,1		



Fig. 5. Bars after testing



Fig. 6. Flaking of corrosion products in the concrete body

2.2 Numerical modeling

Numerical modeling, which replicates experimental tests, was performed in the Ansys software package. The solution was performed in axisymmetric formulation. Concrete and reinforcement modeling was performed using Plane183 (rectangular 8-node FE) with a finite element size of 1x1mm (Fig 7, a), b)).

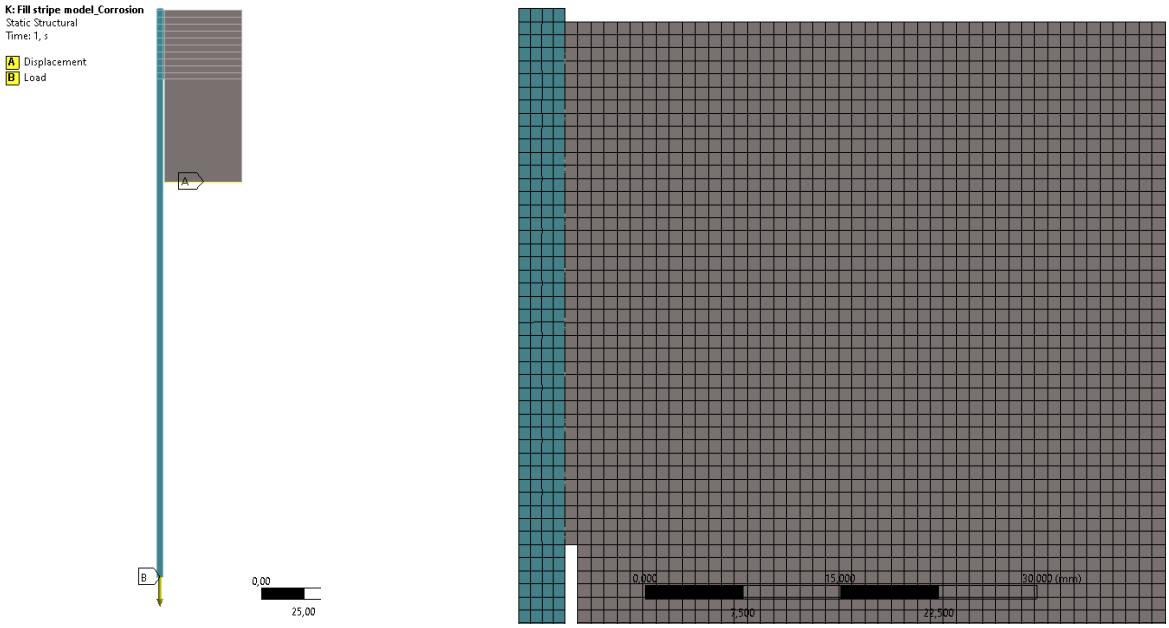

a) b)

Fig. 7. Object of study: a) general view of the model; b) finite element model

The simplest method within the framework of numerical modeling of reinforcement-concrete coupling and subsequent analysis of deformation (fracture) processes when solving contact problems of reinforcement bar pulling out of concrete, are methods that explicitly take into account the non-continuity of concrete-reinforcement coupling [1-2].

The modeling of the non-continuity, i.e., the slippage of the reinforcement relative to the concrete is described by a simplified method that simulates the real processes of jointing reinforcement with concrete. The simplification consists in modeling a smooth reinforcing bar, and its coupling with concrete in the form of nonlinear springs, the stiffness of which is determined on the basis of experimental data.

The nonlinear springs were modeled using the COMBIN39 element. The reinforcement-concrete interface zone was divided into 10 sections, each of which modeled a spring element; this division led to a more correct analysis of the stress-strain state. The first end of the spring was fixed to the reinforcement bar node and the second end to the concrete surface (Fig. 8).

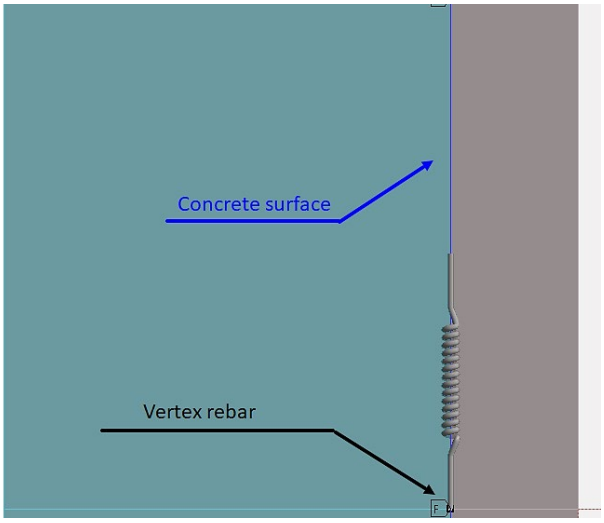

Fig. 8. Spring modeling in the reinforcement-concrete interface zone

The behavior of concrete was described using the Menetrey-Willam model [24], which uses plastic flow theory as its basis. The Menetrey-Willam model is generally more applicable for modeling the behavior of bound aggregates such as concrete than the Drucker-Prager model without modifications [25-26].

This model uses plastic flow theory as a basis. The concrete model consists of three main components:

The three-invariant limit surface fMW described by formula 2:

$$f_{MW} = \frac{c_2}{c_3}\left[\sqrt{2\xi} + rp\right] + p^2 - \frac{1}{c_3}, \tag{2}$$

where, c2 and c3 equation parameters controlling the shape of the meridional cross-section of the surface and determined based on the yield strengths in uniaxial tension (Rt), compression (Rc) and biaxial compression (Rb) [26]. The ultimate surface is shown in Figure 9:

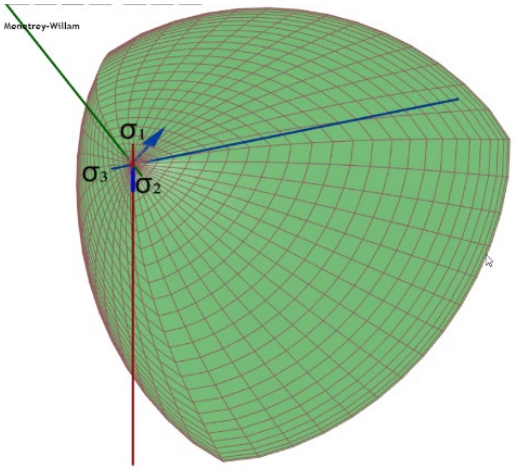

Fig. 9. The limiting surface of the Menetrey-Willam model.

The surface of the plastic potential [24], which is responsible for the direction of the plastic strain vector described by the formula 3:

$$Q_{MW} = \rho^2 + B_g p + C_g \xi, \tag{3}$$

where Bg and Cg are parameters characterizing the plastic potential.

Laws of evolution of the limiting surface, responsible for hardening and de-hardening of the material. The model provides separate evolution laws for compression and tension (see Fig. 10):

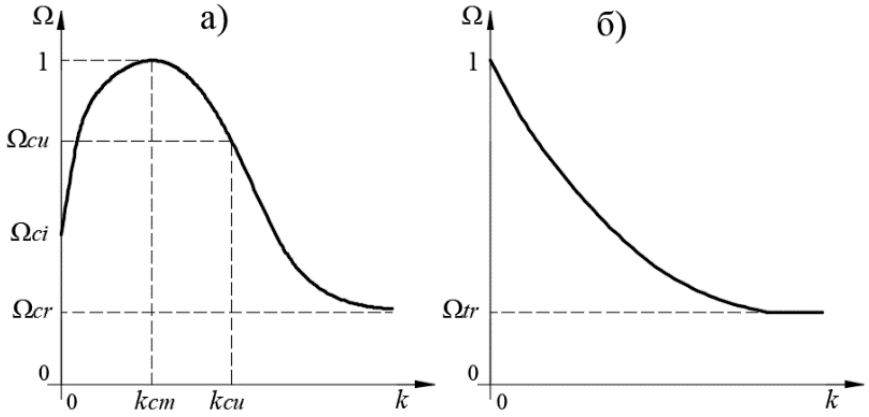

Fig. 10. Graphical interpretation of the laws of evolution of the limiting surface in compression (a) and tension (b).

The strength and deformation characteristics of concrete used in the numerical calculation are determined on the basis of experimental tests, the cubic compressive strength is 32,5 MPa, which corresponds to concrete class B25, hence the tensile strength can be assumed to be 1.55 MPa. To determine the elastic, plastic and total deformations and their corresponding stresses required to set the laws of evolution (Figure 10), according to Appendix D of SP 63.13330 [23], the corresponding values are determined:

- Concrete compressive strength is 18,5 MPa;
- Ωci=0,65 - 18,5x0,65=12,02 MPa;
- Ωcu=0,85 - 18,5x0,85=15,72 MPa;
- Ωcr=0,175 - 18,5x0,175=3,23 MPa;
- Initial modulus of elasticity $\mathrm{E} = \sigma_{0,65}/\varepsilon_{0,65} = 12{,}02/0{,}00059 = 20381{,}3$ MPa;
- Tensile strength of concrete - 1,55 MPa;
- Ωtr=0,1 – 1,55x0,1=0,155 MPa.

The behavior of reinforcing steel is described by bilinear dependence with yield strength of 515MPa, accepted on the basis of the conducted experimental studies (Fig. 11).

The problem was solved in a nonlinear formulation under static loading conditions using the stepwise Newton-Raphson method. The loading of the model was performed by specifying displacements of the lower end of the reinforcing bar, simulating experimental tests. The displacement application was divided into 100 equal sub-steps.

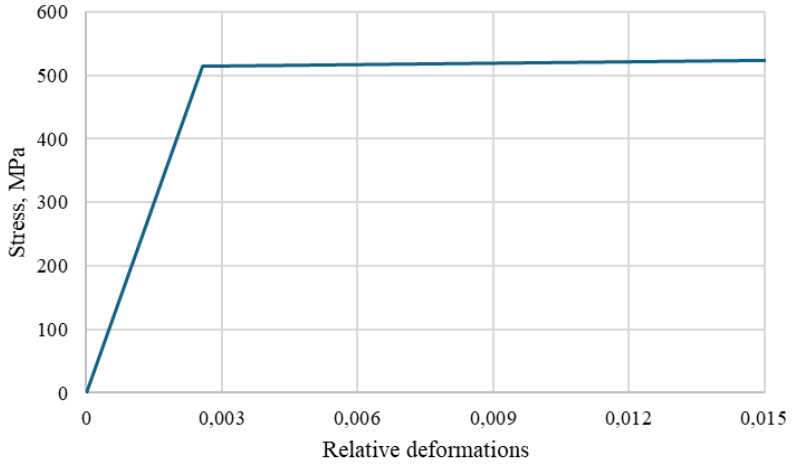

Fig. 11. Bilinear diagram of reinforcement deformation

Spring stiffness in corrosion-damaged and undamaged models was determined based on the results of experimental studies. Spring stiffness is determined by the dependence of the acting pull-out load on the displacement of the upper end of the rod. Assuming the equality of springs in the whole section of bond between reinforcement and concrete, the stiffness of each spring can be determined by the formula 4:

$$D(s) = \frac{F}{n \cdot s} \tag{4}$$

where F is the value of the force applied to the rod; n is the number of springs; s is the displacement of the upper end of the rod.

In calculations, the spring parameters were given by the exponential dependence obtained on the basis of experimental tests, shown in Figure 4.

3 Results and discussions

A constant displacement of 1,5 mm was set to the lower end of the rod. The calculation results corresponding to the peak load for the corrosion-damaged and undamaged model are shown in the figure 12, where the vertical displacement of the rod relative to the concrete section is observed and the characteristic picture of stress distribution along the contact.

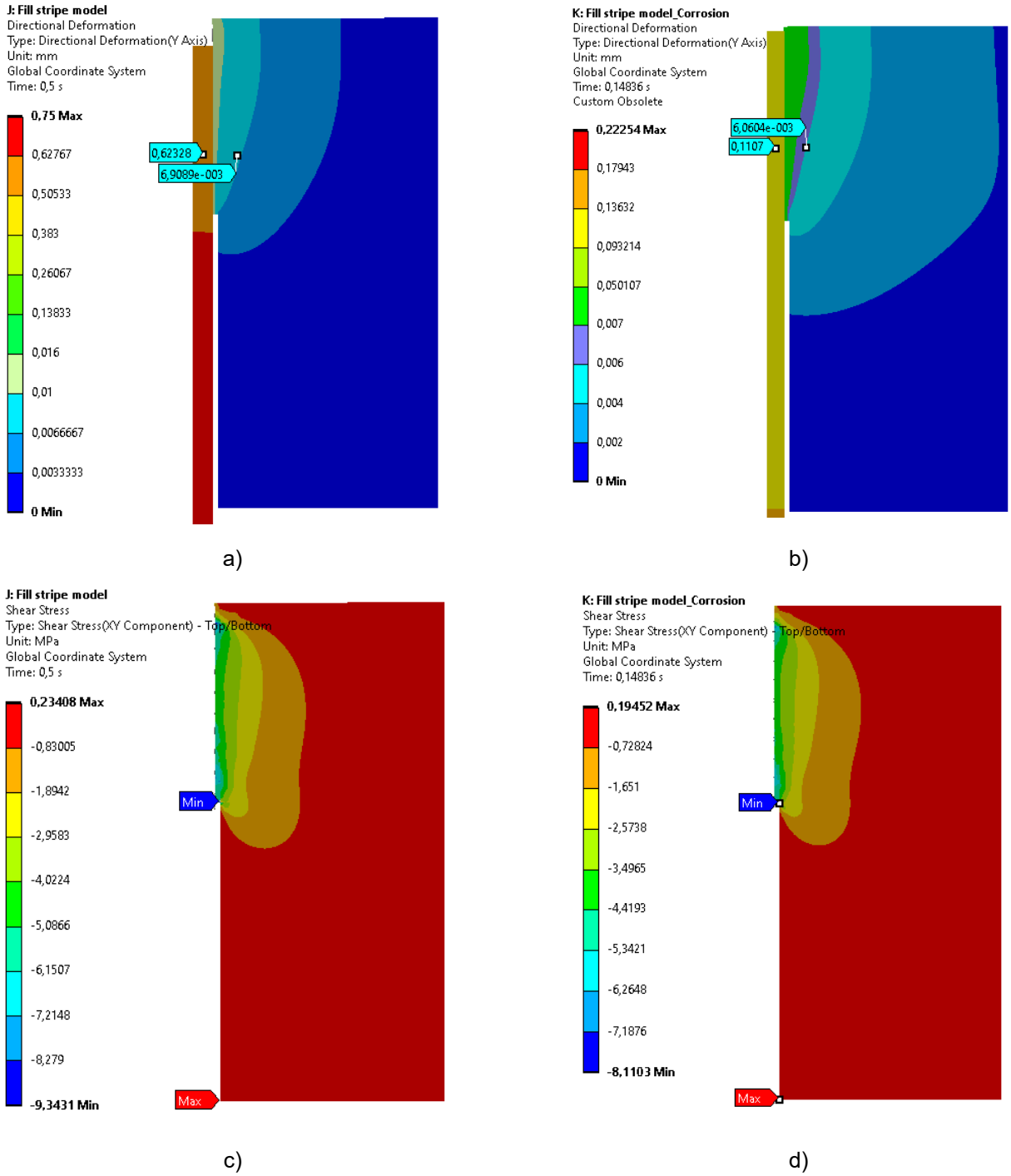

Fig. 12. Isopoles of vertical displacements and tangential stresses in concrete of undamaged (a and c) and corrosion-damaged (b and d) models

Figure 13 shows a graphical comparison of the reaction force dependence on the displacement of the upper and lower ends of the reinforcement. There is a significant difference in the displacements between the ends of the reinforcement, which shows the presence of deformation of the rod, despite the fact that the modulus of elasticity of steel is significantly greater than the modulus of elasticity of concrete, which indicates the inadmissibility in such problems to consider the rod as an absolutely rigid body.

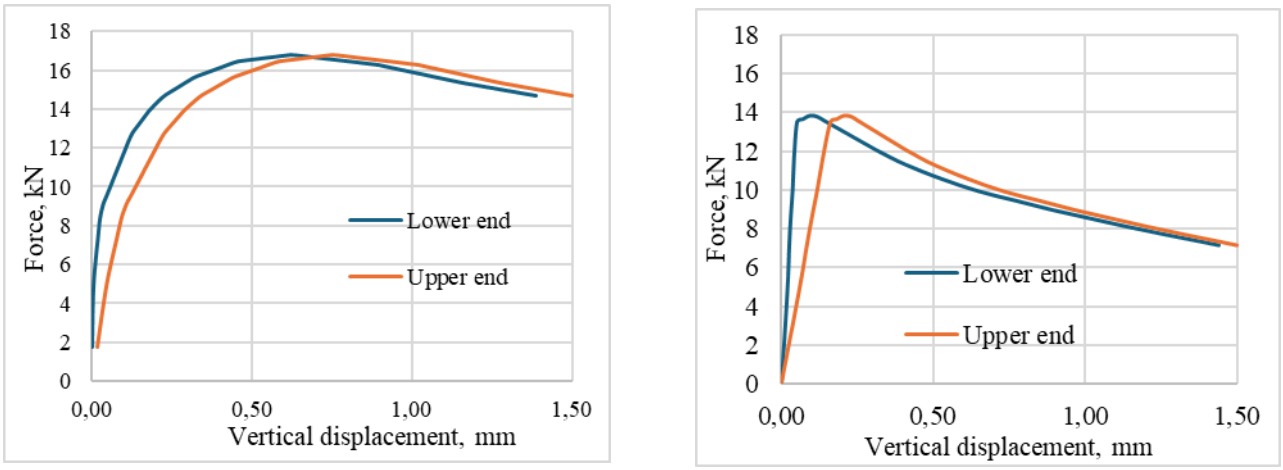

Fig. 13. Comparison of pull-out force from displacement of the lower and upper ends of corroded (a) and undamaged rod (b)

Thus, the difference in displacement of the lower and upper ends of the undamaged and corrosion-damaged rod is 20% (0.62mm and 0.75mm) and 115% (0.093mm and 0.2mm), respectively. The difference between the displacement of the lower end of the undamaged and damaged rod is 6.6 times (0.62mm and 0.093mm) and the upper end is 3.75 times (0.75mm and 0.2mm). The obtained results show that the presence of corrosion damage leads to degradation of bonding forces and as a result to reduction of deformation of reinforcing bars and tensile forces occurring in them.

The values of ultimate pull-out force at 22% corrosion damage of reinforcing bars decreases by 17%, hence the presence of corrosion damage of reinforcing bars leads not only to known and to some extent studied negative consequences such as destruction of the concrete cover of concrete, reduction of bearing capacity, but also to hidden negative consequences, such as failure to provide the required anchorage length, which does not guarantee the joint work of concrete and reinforcement and may lead to slippage of reinforcement in the body, which will lead to transformation of the static work of the structure, a different redistribution of internal forces and change the stress-strain state of the designed structure.

4 Conclusions

- The test results determined a 6.05% reduction in bond of the corroded bar relative to the undamaged bar, with a percentage of reinforcement corrosion over the cross-sectional area of 23.08%.
- The maximum stresses in the reinforcement in the corrosion damaged bar are higher by 6.84% than in the undamaged bar. This effect is achieved by reducing the area of the reinforcement, taking into account a slight decrease in the maximum load on the specimen.
- From the deformation graphs, the effect of corrosion products on the performance of the bar in the concrete body is noticeable. Corrosion damaged reinforcement is held in the concrete by the friction of the rod against the corrosion products and the graph becomes linear. If there is no damage to the reinforcement, plastic deformations of concrete between the profile of the reinforcement can be seen as it works to pull out of the concrete.
- The use of numerical method of calculation of adhesion of corrosion-damaged reinforcement with concrete by means of a set of nonlinear springs allows to correctly analyze and describe the dependences of adhesion forces on displacement.
- To obtain more reliable data on the effect of corrosion on the bonding of reinforcement to concrete, a comprehensive study including different diameters of reinforcement, different percentages of corrosion, relative anchorage lengths, and different strength classes of concrete is needed.

5 Acknowledgements

The authors of the article express their gratitude to the laboratory of testing building materials, products and structures for the opportunity to conduct experimental studies on the basis of technical equipment of the laboratory. And also

to the employee of the unit Kovalev Mikhail for all-round assistance and support and Vasyutin Vladimir for the preparation of experimental samples.

6 References

[1] Benin, A. V., Semyonov, A. S., Semyonov, S. G., & Melnikov, B. E. (2012). Finite-element modeling of fracture processes and resource estimation of the highway bridge elements taking into account the corrosion damage. *Magazine of Civil Engineering, 7*(33), 32–42.

[2] Benin, A. V., Semenov, A. S., Semenov, S. G., & Melnikov, B. E. (2013). Mathematical modeling of the process of fracture of bonding of reinforcement with concrete. Part 1. Models taking into account non-continuity of the connection. *Magazine of Civil Engineering, 5*(40), 86–99.

[3] Benin, A. V., Semenov, A. S., Semenov, S. G., & Melnikov, B. E. (2014). The simulation of bond fracture between reinforcing bars and concrete. Part 2: Models without taking the bond discontinuity into account. *Magazine of Civil Engineering, 45*(1), 23–40.

[4] Kholmianskiy, M. M. (1981). *Kontakt armatury s betonom* [Contact between concrete and reinforcement]. Stroyizdat.

[5] Shima, H., Chou, L.-L., & Okamura, H. (1987). Micro and macro models for bond in reinforced concrete. *Journal of the Faculty of Engineering: University of Tokyo, 39*(2), 133–194.

[6] Balázs, G. L. (2007). Connecting reinforcement to concrete by bond. *Beton- und Stahlbetonbau, 102*, 46–50.

[7] Comité Euro-International du Béton. (1993). *CEB-FIP Model Code 1990: Design code*. Thomas Telford.

[8] Cruz, J. S., & Barros, J. (2004). Modeling of bond between near-surface mounted CFRP laminate strips and concrete. *Computers and Structures, 82*, 1513–1521.

[9] Rehm, G. (1957). The fundamental law of bond. In *Proceedings of the Symposium on Bond and Crack Formation in Reinforced Concrete* (pp. 491–498). Stockholm.

[10] Wu, Y. F., & Zhao, X. M. (2012). Unified bond stress-slip model for reinforced concrete. *Journal of Structural Engineering, 139*(11), 1951–1962.

[11] Lee, H. S., Noguchi, T., & Tomosawa, F. (2002). Evaluation of the bond properties between concrete and reinforcement as a function of the degree of reinforcement corrosion. *Cement and Concrete Research, 32*(8), 1313–1318.

[12] Cabrera, J. G. (1996). Deterioration of concrete due to reinforcement steel corrosion. *Cement and Concrete Composites, 18*(1), 47–59.

[13] Stanish, K. D., Hooton, R. D., & Pantazopoulou, S. J. (1999). Corrosion effects on bond strength in reinforced concrete. *ACI Structural Journal, 96*(6), 915–921.

[14] Yuan, Y., Yu, S., & Jia, F. (1999). Deterioration of bond behavior of corroded reinforced concrete. *Industrial Construction, 29*(11), 47–50. (In Chinese.)

[15] Auyeung, Y., Balaguru, P., & Chung, L. (2000). Bond behavior of corroded reinforcement bars. *ACI Materials Journal, 97*(2), 214–220.

[16] Chung, L., Cho, S. H., Kim, J. H. J., & Yi, S. T. (2004). Correction factor suggestion for ACI development length provisions based on flexural testing of RC slabs with various levels of corroded reinforcing bars. *Engineering Structures, 26*(8), 1013–1026.

[17] Chung, L., Kim, J. H. J., & Yi, S. T. (2008). Bond strength prediction for reinforced concrete members with highly corroded reinforcing bars. *Cement and Concrete Composites, 30*(7), 603–611.

[18] Bhargava, K., Ghosh, A. K., Mori, Y., & Ramanujam, S. (2008). Suggested empirical models for corrosion-induced bond degradation in reinforced concrete. *Journal of Structural Engineering, 134*(2), 221–230.

[19] Kivell, A. R. L. (2012). *Effects of bond deterioration due to corrosion on seismic performance of reinforced concrete structures*. University of Canterbury.

[20] Lin, H. W., & Zhao, Y. X. (2016). Effects of confinements on the bond strength between concrete and corroded steel bars. *Construction and Building Materials, 118*, 127–138.

[21] ACI Committee 318. (2002). *Building code requirements for structural concrete (ACI 318-02) and commentary (318R-02)*. American Concrete Institute.

[22] Tian, Y., Liu, J., Xiao, H., Zhang, Y., Mo, Q., Shen, J., & Shi, J. (2020). Experimental study on bond performance and damage detection of corroded reinforced concrete specimens. *Advances in Civil Engineering, 2020*, Article 7658623. https://doi.org/10.1155/2020/7658623

[23] SP 63.13330.2018. (2018). *Concrete and reinforced concrete structures: Basic provisions. SNiP 52-01-2003 (with Amendment No. 1)*. Code of Regulations.

[24] Dmitriev, A., Novozhilov, Y., Mikhalyuk, D., & Lalin, V. (2020). Calibration and validation of the Menetrey-Willam constitutive model for concrete. *Construction of Unique Buildings and Structures, 88*, 84–91.

[25] Korsun, V. I., Karpenko, S. N., Makarenko, S. Y., & Nedoresov, A. V. (2021). Modern strength criteria for concrete under triaxial stress states. *Building and Reconstruction*, (5), 16–30. https://doi.org/10.33979/2073-7416-2021-97-5-16-30

[26] fib. (2013). *Model code for concrete structures 2010*. International Federation for Structural Concrete.

7 Conflict of interest statement

The authors declare that they have no conflicts of interest.

8 Author contributions

Dmitriy Popov: conceptualization, supervision, methodology, visualization, writing-original draft preparation, validation, resources; Maksim Kudryavtsev: investigation, data curation, formal analysis, writing, reviewing.

9 Availability statement

There is no dataset associated with the study or data is not shared.

10 Supplementary materials

There are no supplementary materials to include.

Paper submitted: 03.12.2025.
Paper accepted: 31.07.2026.
This is an open access article distributed under the CC BY 4.0 terms and conditions